Cellulose (2019) 26:5621–5633
https://doi.org/10.1007/s10570-019-02492-z

ORIGINAL RESEARCH

Preparation, characterization and antibacterial properties of cellulose membrane containing N-halamine

Shengli Zhang · Chengcheng Kai · Bofang Liu · Silue Zhang · Wei Wei · Xiaoling Xu · Zuowan Zhou

Received: 2 April 2019 / Accepted: 6 May 2019 / Published online: 11 May 2019

Abstract Polyethylenimine (PEI), a type of water-soluble chain polymer containing a great number of primary, secondary and tertiary amine groups in the molecule, was used as an N-halamine precursor. It was grafted onto dialdehyde cellulose membrane (DCM) followed by chlorination to prepare a novel N-halamine antibacterial cellulose membrane (Cl–PEI–DCM). The appropriate conditions affecting the aldehyde content of DCM and the active chlorine (Cl^+) content of Cl–PEI–DCM were systematically studied at oxidation, grafting and chlorination stages, respectively. The structure and properties of the samples were investigated by SEM, ATR–FTIR, XRD, XPS, light transmittance measurements and tensile tests. The stability and rechargeability of the Cl–PEI–DCM were evaluated, and its antibacterial activity was tested against *S. aureus* and *E. coli*. Results showed that the Cl^+ content of the chlorinated samples was strongly dependent on the aldehyde content of DCM and PEI concentration. Under the optimum testing condition, the Cl^+ content of the Cl–PEI–DCM reached 1.30 wt%. The hydroxyl groups on the cellulose membrane were changed to aldehyde groups and the successful introduction of PEI and N–Cl bond were confirmed. The 1.30 wt% Cl–PEI–DCM exhibited high antibacterial activity against both *S. aureus* and *E. coli*, which can completely inactivate two bacterial pathogens within 5 min even after 15 days of storage. Moreover, the Cl–PEI–DCM membrane displayed good stability, rechargeability, transparency and high mechanical strength. These results demonstrated that the Cl–PEI–DCM can be considered as a visualized wound dressing material or antibacterial shoe insole.

S. Zhang (✉) · C. Kai · B. Liu · S. Zhang
School of Geosciences and Environmental Engineering, Southwest Jiaotong University, Chengdu 610031, Sichuan, China
e-mail: zhang222@home.swjtu.edu.cn

W. Wei · X. Xu · Z. Zhou (✉)
School of Materials Science and Engineering, Southwest Jiaotong University, Chengdu 610031, Sichuan, China
e-mail: zwzhou@swjtu.edu.cn

Graphical abstract

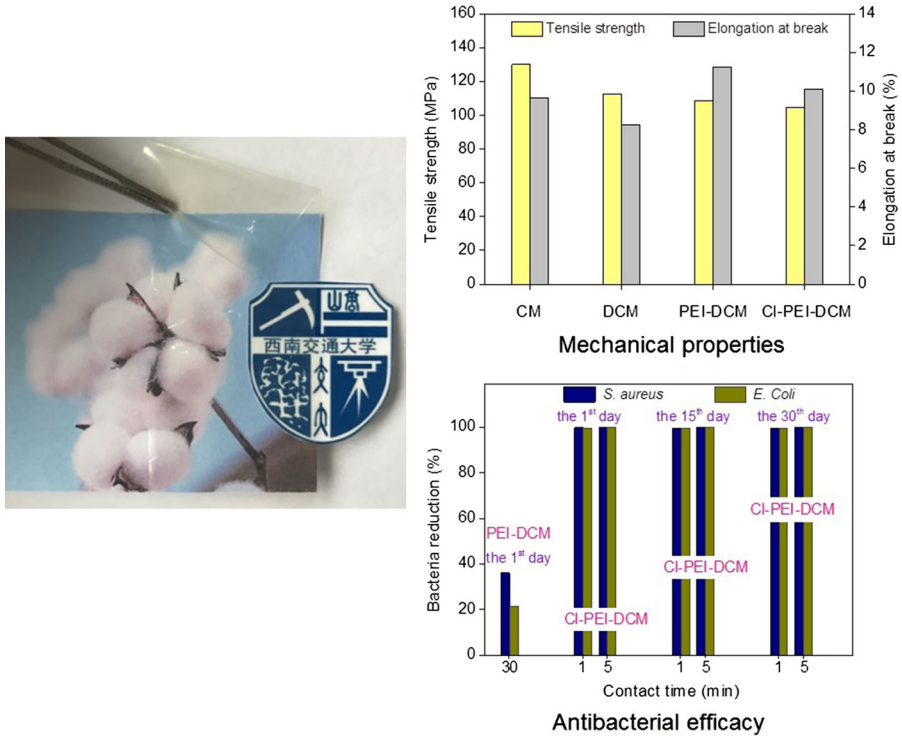

Keywords Periodate oxidation · Dialdehyde cellulose · Polyethylenimine (PEI) · Antibacterial cellulose membrane · N-chloramine

Introduction

As the increasing threat of microorganisms on environment and human health, antibacterial materials have achieved extensive attention (Toure et al. 2014; Shankar and Rhim 2018). Various antibacterial agents, including nanoparticles of noble metals and metal oxides (Wang et al. 2017b; Qi et al. 2017), quaternary ammonium compounds (Gerba 2015; Chen et al. 2019), chitosan (Cheung et al. 2015; Chen et al. 2016) and N-halamines (Demir et al. 2017; Dong et al. 2017), are widely used over the years. Among them, N-halamines have demonstrated many advantages such as rapid inactivation against a broad spectrum of microorganisms in brief contact times, safety to humans and environment, regenerability as well as low cost (Hui and Debiemme-Chouvy 2013; Liu et al. 2015).

Currently, the reported N-halamine precursors focus on cyclic structure compounds with secondary amine groups (Hou et al. 2017; Wang et al. 2017a). Polyethylenimine (PEI), a type of water-soluble chain polymer, contains a great number of primary, secondary and tertiary amine groups in the molecule. It can be used as a potential N-halamine precursor. Moreover, PEI of lower molecular weights exhibits minimal toxicity (Parhiz et al. 2013). A series of investigation on PEI as chelator of heavy metal ions, cell-attachment promoter, gene and DNA vaccine delivery reagent, and others have been performed (Li et al. 2014; Zhang et al. 2018; Ciofani et al. 2008; Sheppard et al. 2014). To our knowledge, the only work reported to date concerning PEI-based N-halamine antibacterial material has originated from the laboratory of Goddard and coworkers (Bastarrachea and Goddard 2013). They attached the branched PEI coatings to the surface of stainless steel by layer deposition technique. After chlorination, the obtained N-halamine-modified stainless steel produced about a

1.5 log inactivation of *Listeria* monocytogenes at a contact time of 6 h.

Cellulose, the most abundant natural polymer in the world, is highly attractive due to renewability, nontoxicity, biodegradability, biocompatibility and low price (Roy et al. 2009). It has been widely applied in many fields such as textile, paper-making, pharmaceutics and cosmetics. However, cellulose itself has no antibacterial property and is easy to breed bacteria in use (Gu et al. 2018). The researches involving antibacterial cellulose have received increasing attention in recent years (Kang et al. 2013; Li et al. 2015; Demircan and Zhang 2017). Generally, unmodified cellulose tends to form intermolecular and intramolecular hydrogen bonds by its hydroxyl groups, limiting the introduction of other active groups. A popular method is periodate-mediated selective oxidation. Periodate can cleave the C2–C3 bond of the glucopyranoside ring under mild aqueous conditions, and produced 2,3-dialdehyde cellulose (DCM) without significant side products (Li et al. 2011). Afterward, a variety of substituent groups like hydrazone derivatives and imines (Schiff bases) can be introduced to the resultant aldehyde groups (Kim et al. 2000). Especially, Schiff bases make the dialdehyde cellulose a valuable intermediate for cellulose-based functional materials (Zhang et al. 2014; Jin et al. 2015).

In the present study, dialdehyde groups were first introduced into cellulose membrane (CM). Then branched polyethylenimine was grafted onto dialdehyde cellulose (DCM) via Schiff base reaction and followed by chlorination to obtain a novel antibacterial cellulose membrane (Cl–PEI–DCM). The appropriate conditions affecting the aldehyde content of DCM and the active chlorine (Cl^+) content of Cl–PEI–DCM were systematically investigated at the oxidation, grafting and chlorination stages. The structure and properties of the samples were characterized by SEM, ATR–FTIR, XRD, XPS, light transmittance measurements and tensile tests. The stability and rechargeability of the Cl–PEI–DCM were evaluated, and its antibacterial activity was challenged against *S. aureus* and *E. coli*.

Experiments

Materials

Cotton pulp cellulose was provided by Bailu Chemical Fiber Group Ltd. (Xinxiang, China), with DP of 550 and 95% α-cellulose. The pulp has been smashed and dried in a vacuum oven (60 °C) for 5 h before dissolution. Tetrabutylammonium hydroxide (TBAH, 15 wt%) solution was provided by Runjing Chemical Co. Ltd. (Zhenjiang, P. R. China). The TBAH solution was concentrated through distillation under reduced pressure (− 98 kPa, 50 °C). The TBAH working solution of desired concentration was prepared diluting its stock solution with deionized water.

Branched polyethylenimine (PEI, molecular weight 600, 99%) was purchased from Shanghai Aladdin Bio-Chem Technology Co., Ltd. Dimethylsulfoxide (DMSO), sodium periodate ($NaIO_4$) and sodium hypochlorite (NaClO, 10% chlorine) were supplied by Chengdu Kelong Chemical Reagent Co. (Chengdu, China).

S. aureus (ATCC 6538) and *E. coli* (ATCC 25922) was provided by Guangdong Institute of Microbiology, P. R. China. All other chemicals and materials used in this study were purchased from commercial sources, and were used without further purification.

Preparation of N-halamine antibacterial cellulose membrane

Cellulose membrane (CM) was prepared according to the method described in our previous paper (Cao et al. 2018). Then 2 g of CM was immersed in a $NaIO_4$ solution with different initial concentrations (0.5–4 g/L). The mixture was placed into a magnetic stirring water bath pot and stirred for different time (15 min–48 h) at given temperature (5–45 °C) in dark. The desired pH (2–8) was adjusted using 1 mol/L NaOH and 1 mol/L HCl. Thereafter, the oxidized CM was washed with distilled water to prepare dialdehyde cellulose membrane (DCM).

The obtained DCM was immersed in a PEI solution with different initial concentrations (0.005–5 wt%). The mixture was stirred for different time (5–240 min) at room temperature. The desired pH (3–11) was adjusted using 1 mol/L NaOH and 1 mol/L HCl. Subsequently, the aminated cellulose membranes were washed with distilled water and dried at 50 °C

in an oven to prepare the N-halamine precursor PEI–DCM.

The PEI–DCM samples were converted to halamine structure by immersing them in a NaClO solution with different initial concentrations (0.05–5 wt%). The mixture was stirred for different time (15–720 min) at room temperature. The desired pH (3–12) was adjusted using 1 mol/L NaOH and 1 mol/L HCl. Subsequently, the chlorinated samples were washed with distilled water and dried at 35 °C in an oven to finally obtain the antibacterial cellulose membrane Cl–PEI–DCM.

At the same time, CM and DCM were dried at 50 °C in an oven to prepare blank and reference samples.

Characterization of samples

The physical morphologies of the CM, DCM, PEI–DCM and Cl–PEI–DCM were observed on a JSM7800F PRIME (JEOL Com., Japan) electron microscope. The samples were coated with a gold film to improve their conductivity and the quality of the SEM image. The surface functional groups of the CM, DCM, PEI–DCM and Cl–PEI–DCM were detected by a FTIR spectroscope (Nicolet 6700, Thermo Fisher Scientific, America). The data in the range of 4000–400 cm^{-1} were recorded with an ATR accessory at a spectral resolution of 4 cm^{-1}. The surface element compositions of the samples were obtained by XPS on an Escalab 250Xi electron spectrometer (Thermo Fisher Scientific, USA) with an Al Kα source. Their crystal structures were determined by X-ray powder diffraction (XRD, PANalytical X'Pert PRO, Holland). The scan was collected in the 2θ range from 5° to 60° using CuKα radiation (λ = 0.15418 nm) operated at 40 kV and 25 mA.

The transparency of the samples prepared at different stages in the wavelength of 300–900 nm was measured by a UV2550 ultraviolet–visible spectrophotometer (SHIMADZU, Japan) with air as the control. Their tensile strength and elongation at break were tested on a universal tensile machine AGS-J (SHIMADZU, Japan) at room temperature (25 °C, 55% RH) according to ASTM:D638. The samples were stretched at a speed of 2 mm/min. The average value of each property was calculated according to 5 parallel tests.

Determination of aldehyde content and active chlorine content

The aldehyde content of DCM was determined by converting the dialdehyde cellulose to oximes via Schiff base reaction with hydroxylamine (Lindh et al. 2014). The related calculation formula is as follows:

$$Aldehyde\ content\ (\mu mol/g) = \frac{30 \times V}{w}$$

where V is the consumed volume (mL) of the methanol solution with 0.03 mol/L of sodium hydroxide, and w is the weight (g) of DCM.

The loaded active chlorine (Cl^+) content on the Cl–PEI–DCM was determined by a standard iodometric/thiosulfate titration (Kang et al. 2016). The detailed procedure can be described as follows: A small membrane sample (about 1.0 g) was suspended in 25 mL acetic acid solution (0.5 wt%). After adding 0.3 g potassium iodide, the reaction was performed in the dark at room temperature for 30 min. Then 1 mL starch solution (0.5 wt%) was added as an indicator. The system was titrated with $Na_2S_2O_3$ (0.005 mol/L) until the blue color disappeared at the end point. The Cl^+ content of the sample is calculated according to the following formula:

$$Cl^+\ (wt\%) = \frac{C \times V \times 35.45}{m \times 2} \times 100$$

where Cl^+ (wt%) is the weight percent of active chlorine on the membrane, C and V stand for the concentration (mol/L) and volume (L) of the consumed $Na_2S_2O_3$ solution in the titration, respectively. And m is the weight (g) of the membrane sample.

Antibacterial test

The antibacterial activity of the PEI–DCM and chlorinated samples was evaluated according to modified AATCC Test Method 100-1999 reported by the earlier literature (Sun et al. 2001). A Gram positive bacteria *S. aureus* and Gram negative bacteria *E. coli* were used as model bacteria. First, the membrane samples were cut into small pieces (ca. 4 cm^2), one piece of which was put in a sterilized container. 100 μL of the aqueous suspension containing 10^6 colony-forming units (CFU)/mL bacteria was added to the center of the membrane, and then another identical membrane was placed on the first membrane surface

for different contact time. Then the entire sandwich was placed into 10 mL of 0.5 wt% sodium thiosulfate solution to neutralize all oxidative chlorine residues and recover survival bacteria. The bacteria suspension was serially diluted, and 100 μL of each dilution was placed onto a nutrient agar plate. The plates were incubated at 37 °C for 24 h, and bacterial colonies were recorded for antibacterial efficacy analysis.

Stability and rechargeability testing

To study the stability of the Cl–PEI–DCM, the samples were stored in a dark environment at ambient temperature. Then the Cl^+ content was tested periodically using the iodometric/thiosulfate titration method for a 30 day storage period.

For the rechargeability test, three dechlorination/chlorination cycles were performed on the Cl–PEI–DCM. In brief, the PEI–DCM membranes were chlorinated under the optimum chlorination conditions and washed with deionized water. After dried at 35 °C in an oven, the Cl^+ content of three samples were determined via an iodometric/thiosulfate titration. The remaining membranes were soaked in a 0.3% $Na_2S_2O_3$ solution at room temperature to quench the active chlorine and then chlorinated again.

Results and discussion

Optimization of $NaIO_4$-oxidation conditions

In the preparation of DCM, the aldehyde content is related to solution pH, $NaIO_4$ concentration, oxidation time and temperature. Meanwhile, the change of aldehyde content has a great influence on the Cl^+ content of the products. Hence, the Cl^+ content was also used as an evaluation index in the optimization of $NaIO_4$-oxidation conditions. Figure 1a presents the impact of solution pH on two indexes with $NaIO_4$ concentration of 1 g/L, oxidation time of 6 h and oxidation temperature of 25 °C. As the pH rose from 2 to 8, the aldehyde content of the obtained DCM firstly increased from 93 to 201 μmol/g and then decreased to 47 μmol/g. The reason was that the oxidation potential of periodate is related to hydrogen ion concentration and periodate acid is difficult to ionize in strong acid solution. At the same time, the Cl^+ content of the resultant samples increased rapidly from 0.57 to 0.77 wt% with raising the pH from 2 to 3, and then gave a small change at the pH range of 3–5. Afterward, further raising the pH to 8, the Cl^+ content sharply decreased to 0.29 wt%. Thus $NaIO_4$ solution was kept at natural pH (ca. 5.3) for the follow-up experiments.

Figure 1b shows the effects of oxidation temperature on the aldehyde content and Cl^+ content. It is clear that there existed a linear correlation between the aldehyde content and oxidation temperature. As the oxidation temperature rising from 5 to 45 °C, the aldehyde content of DCM continuously increased from 12 to 353 μmol/g. However, the Cl^+ content showed an obvious decrease after reaching the maximum value of 0.91 wt% at 30 °C. It was because that aldehyde content would impact the introduction of PEI. For the subsequent study, the oxidation of CM was carried out at room temperature (25 °C).

Figure 1c, d show the influence of $NaIO_4$ concentration and oxidation time on the aldehyde content and Cl^+ content. It was evident that prolonging oxidation time or increasing $NaIO_4$ concentration, the aldehyde content gave a constant increase. By contrast, the Cl^+ content of Cl–PEI–DCM showed a different trend which increased sharply at first and then gradually decreased with delaying oxidation time. Furthermore, the time to reach the optimal value expanded with reducing $NaIO_4$ concentration. These results indicated that the Cl^+ content of the chlorination samples was strongly dependent on the aldehyde content of DCM. When the aldehyde content was too low, only a little PEI was grafted on the surface of cellulose membrane. Improving the aldehyde content can increase the grafting amount of PEI, but on the other hand, the aldehyde groups could reacted with multiple primary amino groups of PEI molecules, causing the decrease of the available N–H bonds at chlorination stage. Therefore, a controlled amount of aldehyde content was necessary in order to prepare antimicrobial cellulose membrane with higher Cl^+ content. In consideration of cost and time, $NaIO_4$ concentration and oxidation time were fixed at 1 g/L and 6 h, respectively.

Optimization of PEI-grafting conditions

Because it is difficult to measure the grafting amount of PEI on the DCM, the Cl^+ content of the products was adopted as the evaluation index for optimizing the

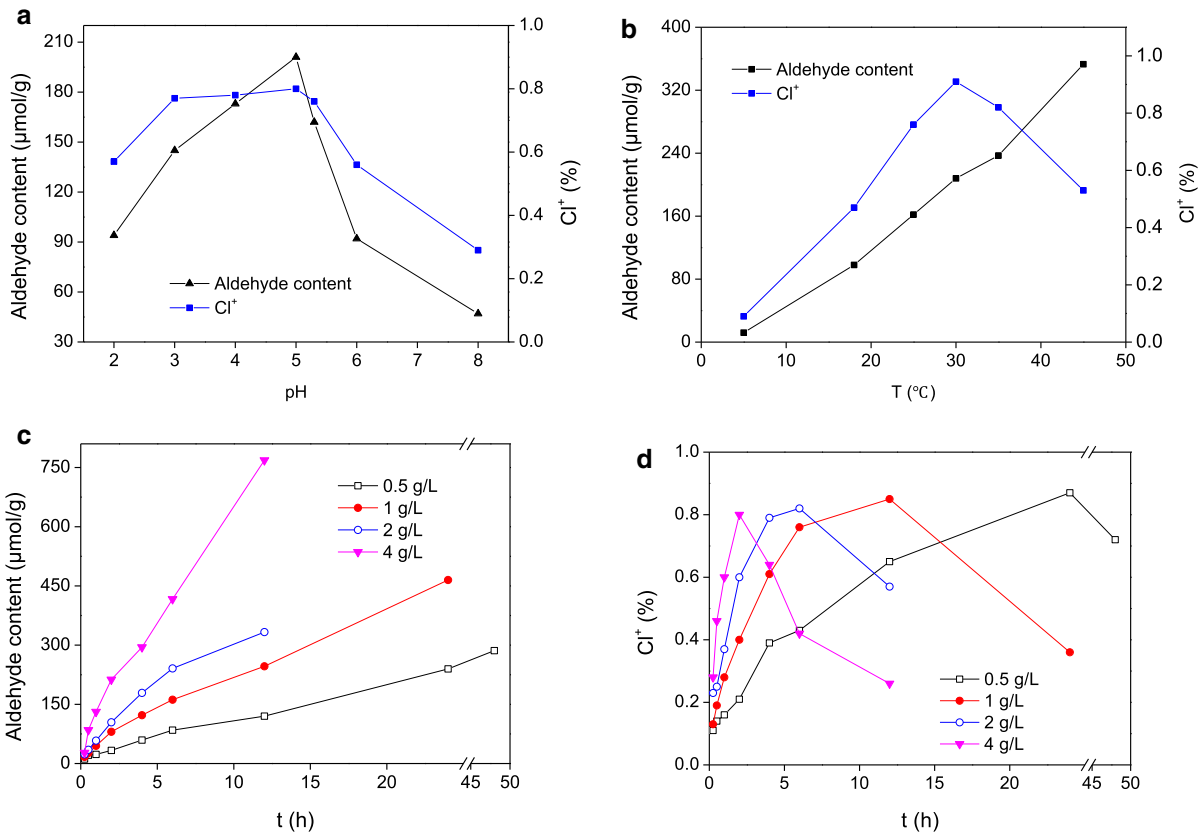

Fig. 1 Effects of solution pH (**a**), oxidation temperature (**b**) and oxidation time at different $NaIO_4$ concentrations (**c**, **d**) on the aldehyde content of DCM and the Cl^+ content of Cl–PEI–DCM at oxidation stage (PEI-grafting conditions: 0.05 wt% PEI solution at natural pH, reaction time of 2 h at room temperature; chlorination conditions: 2.5 wt% NaClO solution at pH 8, chlorination time of 2 h at room temperature)

PEI-grafting conditions as depicted in Fig. 2. From Fig. 2a, it is clear that the Cl^+ content increased from 0.05 to 0.76 wt% as increasing the solution pH from 3 to 10.3 and then decreased with the further rise of pH. Hence, the natural pH 10.3 is adopted for the subsequent experiments. This suggested that alkaline condition was beneficial to the Schiff base reaction between PEI and DCM. The possible reasons were as follows: (1) the amino groups on PEI are easy to protonize under low pH, which is not conducive to the Schiff base reaction. (2) The self-condensation of aldehyde groups could happen at too high basicity, dropping the grafting amount of PEI. When increasing the grafting time from 5 to 240 min, the Cl^+ content firstly increased from 0.22 to 0.76 wt% and then decreased. It was expected because prolonging reaction time, the reactive aldehyde groups were consumed continuously. Therefore, 120 min was chosen as the appropriate grafting time.

Figure 2b shows the effect of PEI concentration on the Cl^+ content with DCM of different aldehyde content used. It can be seen that the Cl^+ content increased at the beginning, especially yielding a big jump when PEI concentration changed from 0.01 to 0.05 wt%, and then gave a decrease. This could be attributed to the fact that PEI is a flexible chain macromolecule and its molecular conformation is affected by PEI concentration in aqueous solution. The "random coil" state of PEI molecular chain extended in an extremely dilute solution, and interwove even twined with increasing the PEI concentration. This had an important influence on the reaction between the amino groups of PEI and the aldehyde groups of DCM. Therefore, the PEI concentration was fixed at 0.05 wt% in sequence experiments. For the given

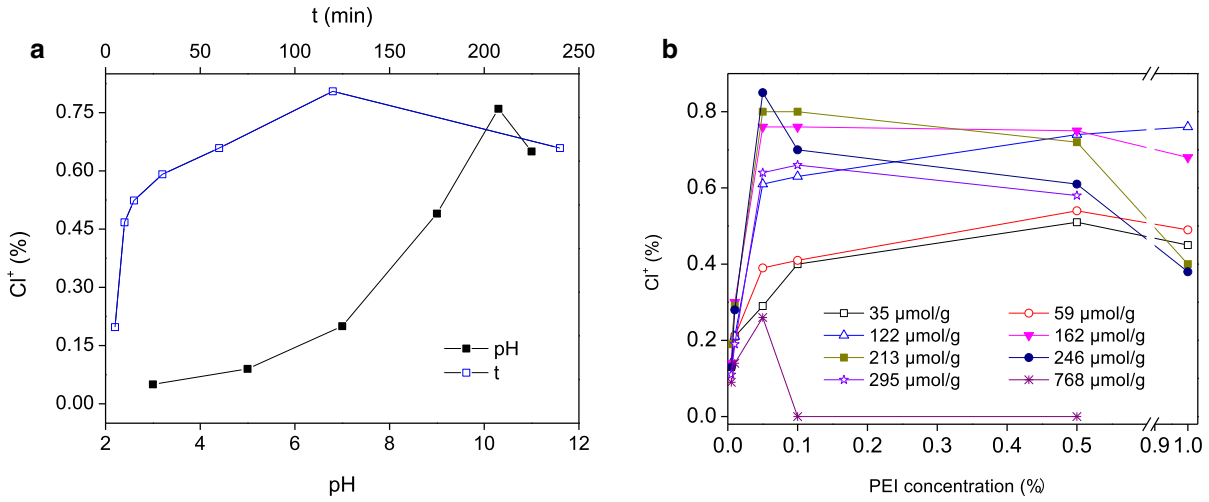

Fig. 2 Effects of solution pH (**a**), reaction time (**a**) and concentration PEI with DCM of different aldehyde content used (**b**) on the Cl^+ content of Cl–PEI–DCM at grafting stage (oxidation conditions: 1 g/L $NaIO_4$ solution at natural pH, oxidation time of 6 h at 25 °C; chlorination conditions: 2.5 wt% NaClO solution at pH 8, chlorination time of 2 h at room temperature)

PEI concentration, the change trend of the Cl^+ content was in accordance with the result obtained in "Optimization of $NaIO_4$-oxidation conditions" section.

Effects of the chlorination parameters

Figure 3 shows the effects of solution pH, chlorination time and NaClO concentration on the Cl^+ content of Cl–PEI–DCM at chlorination stage. It can be observed that the Cl^+ content increased slowly from 1.18 to 1.33 wt% with the pH rising from 3 to 6, and then decreased rapidly to 0.06 wt% with the further increase of solution pH (Fig. 3a). Hence, acidic condition was good for the chlorination reaction of PEI–DCM. This is because the ratios of Cl_2, HOCl, and OCl^- in solution are pH dependent (Deborde and von Gunten 2008). And the established chlorinating strength of these species is $Cl_2 \sim HOCl > OCl^-$

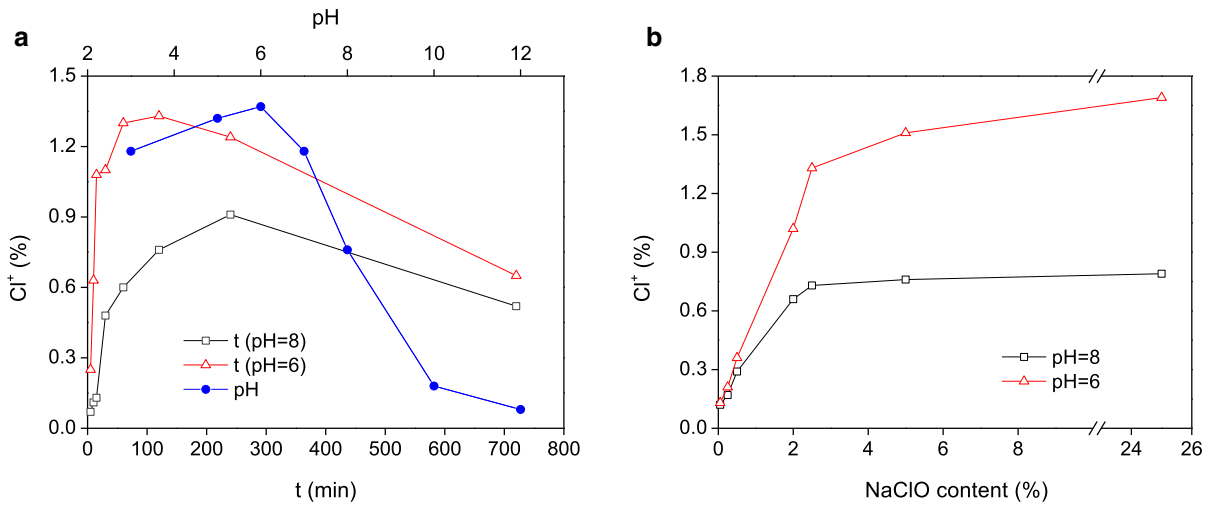

Fig. 3 Effects of solution pH (**a**), chlorination time under different pH conditions (**a**) and NaClO concentration under different pH conditions (**b**) on the Cl^+ content of Cl–PEI–DCM at chlorination stage (oxidation conditions: 1 g/L $NaIO_4$ solution at natural pH, oxidation time of 6 h at 25 °C; PEI-grafting conditions: 0.05 wt% PEI solution at natural pH, reaction time of 2 h at room temperature)

(Soice et al. 2003). When pH is below 2, Cl_2 is the major species. Between pH 2 and 7.5, HOCl predominates. At pH greater than 7.5, the majority is OCl^-, and the solution is fairly stable above pH 12 where HOCl is almost nonexistent.

The effects of chlorination time and NaClO concentration on the Cl^+ content under different pH conditions (6 and 8) were presented in Fig. 3a, b, respectively. Though the chosen pH is different, the Cl^+ content in the products gave the similar trend which increased at first and then decreased with chlorination time expanded. The higher Cl^+ content can be found for the reaction system of pH 6 and the time to reach the maximum value was shorter. However, the same Cl^+ content cannot be obtained for pH 8 even though the chlorination time was increased. The related mechanism remains to be studied. From Fig. 3b, it was obvious that the Cl^+ content rapidly increased at first and then slowed down with increasing the NaClO concentration. It was ascribed to the fact that HClO was more stable in dilute solution, resulting that less N–H was switched to N–Cl. For the fixed PEI–DCM, the total available N–H was limited and too high NaClO concentration gave no additional contribution for the Cl^+ content. In addition, increasing NaClO concentration cannot compensate the effect caused by solution pH. Thereby, the chlorination conditions recommended were NaClO concentration of 2.5 wt%, solution pH of 6, chlorination time of 1 h at room temperature, where the Cl^+ content was 1.30 wt%.

Characterization of the samples

FTIR spectra were recorded to identify the functional groups on the samples obtained at different stages, and the results were showed in Fig. 4a. In the CM spectrum, the strong adsorption at 3350 cm^{-1} was due to the O–H stretching vibration. The bands in the range from 3000 to 2800 cm^{-1} were ascribed to the C–H stretching vibration. The peak at 1642 cm^{-1} was principally contributed by the absorbed water, and the small bands in the range of 1450–1200 cm^{-1} were attributed to the C–H and O–H deformation vibrations. The prominent band at 1160 cm^{-1} was assigned to glycosidic linkages between the sugar units while the sharp peak at 895 cm^{-1} corresponded to the ring stretching of glucose. The strong absorption between 1100 and 900 cm^{-1} were attributed to the C–OH deformation vibrations and/or C–O stretching vibrations in cellulose. After $NaIO_4$ oxidation, a characteristic peak at 1738 cm^{-1} can be founded for DCM, corresponding to the vibration of C=O bond. This feature indicated that cellulose was successfully oxidized by $NaIO_4$, and the hydroxyl groups on the cellulose membrane were partially changed to aldehyde groups. But the peak at 1738 cm^{-1} was weak because the dialdehyde groups formed the hemialdal and hemiacetal structures (Varma et al. 1997).

After grafting PEI, two new adsorption peaks appeared at 1575 and 1542 cm^{-1}, which were attributed to the bend vibration of N–H in primary amino and secondary amino groups. The peak at 1642 cm^{-1} became stronger, which was related to the C=N formation in the grafting process. Meanwhile, the adsorption peak locating at 3350 cm^{-1} became stronger and broader, which was attributed to the overlapping of N–H and O–H stretching vibration. The increased intensity at 1060 cm^{-1} was ascribed to the C–N stretching. In addition, the C–H stretching vibration showed an obvious enhancement. All these confirmed that PEI was successfully grafted to the surface of the DCM.

After chlorination in NaClO solution, the absorption bands displayed either an obvious shift or reduction. The bands at 1575 and 1542 cm^{-1} disappeared, suggesting that the N–H bonds were transformed into N–Cl bonds. The reduced absorption at 1642 cm^{-1} was related to the oxidation of C=N double bonds. Meanwhile, the stretching vibration band at 3350 cm^{-1} got weaker. One reason was that the amino groups participated in the chlorination reaction. The other could be that hydroxyl groups of cellulose membrane were oxidized by NaClO.

To further verify the chemical reactions taking place in the preparation, XPS was used to analyze the surface chemical composition of the CM, DCM, PEI–DCM and 1.30 wt% Cl–PEI–DCM. Figure 4b shows the XPS survey spectra in the 0–1000 eV binding energy region. Two strong peaks were observed at 285 and 532 eV for all the samples, which belonged to the binding energies of C 1*s* and O 1*s*, respectively. Compared with CM, the relative contribution of O 1*s* band increased from 15.23 to 21.13% after $NaIO_4$ oxidation, and then decreased to 14.04% after grafting PEI. The opposite change was attributed to the formation and consumption of aldehyde groups. Meanwhile, the N1*s* peak with binding energy at

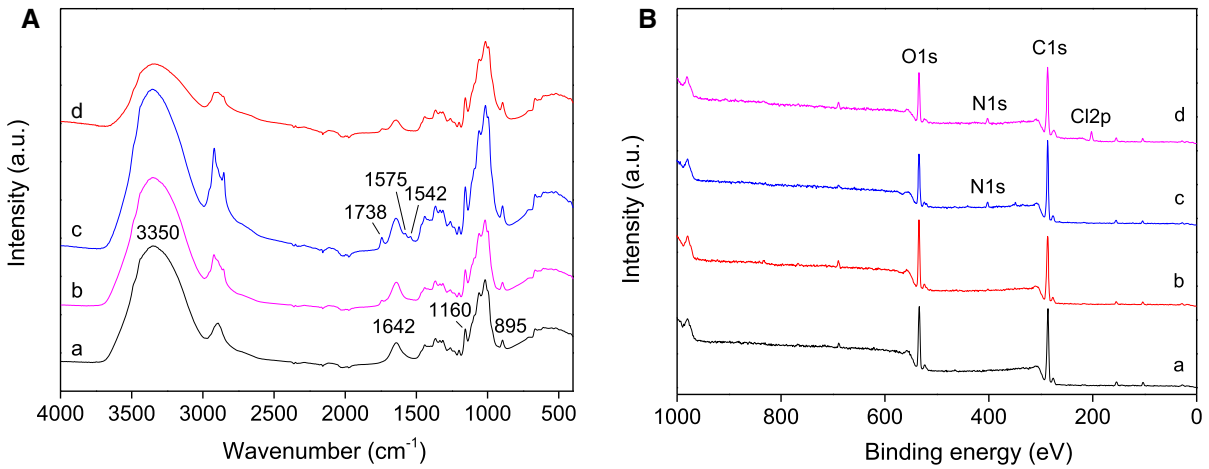

Fig. 4 FT-IR spectra (**A**) and XPS wide scan spectra (**B**) of the CM (a), DCM (b), PEI–DCM (c) and 1.30 wt% Cl–PEI–DCM (d)

399.8 eV can be observed for the PEI–DCM, indicating that PEI molecules were successfully grafted onto the surface of DCM. For the Cl–PEI–DCM, a new peak corresponding to the binding energy of Cl 2*p* can be observed clearly at 200.3 eV, indicating that the chlorination process was successful.

The SEM images of the CM, DCM, PEI–HOCM and 1.30 wt% Cl–PEI–DCM were depicted in Fig. 5. An evident change can be found from the surface morphologies of the samples. The CM had a coarser surface with more cracks. After oxidation to DCM, the cracks on the surface showed a slight decrease, suggesting that the oxidation process had a small effect on the membrane structure. After grafting PEI, the PEI–DCM surface became relatively homogeneous and dense, revealing that the introduction of macromolecular chains improved the membrane structure. After chlorination treatment, the Cl–PEI–

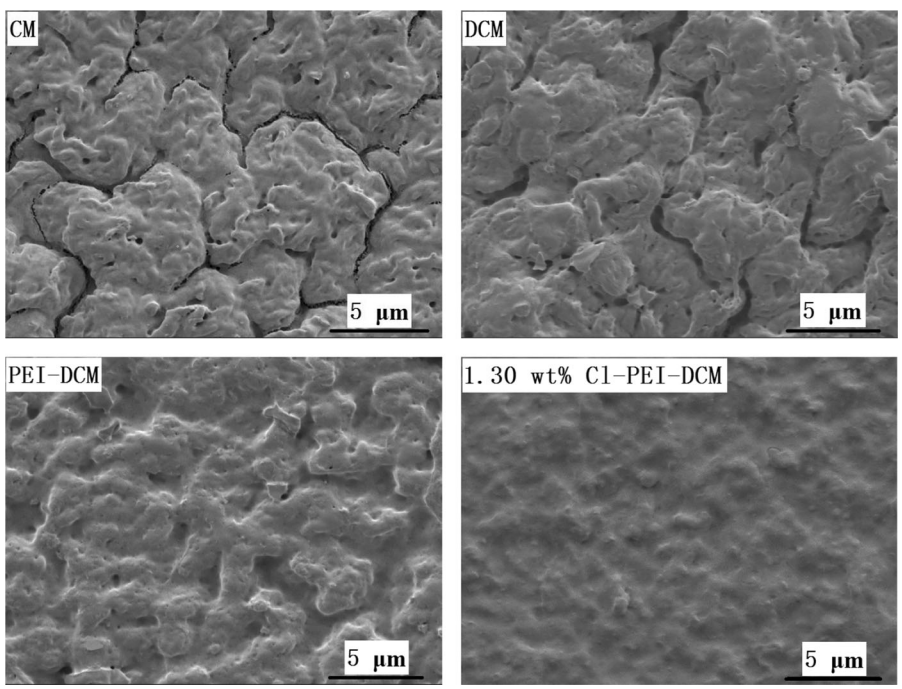

Fig. 5 SEM images of the CM, DCM, PEI–DCM and 1.30 wt% Cl–PEI–DCM

DCM surface further became denser and smoother, which was related to the modification of N-halamine.

The XRD patterns of the CM, DCM, PEI–DCM and 1.30 wt% Cl–PEI–DCM were presented in Fig. 6. According to our previous work (Cao et al. 2018), the cellulose II and cellulose IV crystal structure coexisted in the CM. The DCM and Cl–PEI–DCM had similar XRD pattern with the CM, which demonstrated that the $NaIO_4$ oxidation and chlorination treatment had a small influence on the crystallinity of cellulose membrane.

The transparency of the samples obtained at different stages was measured in the wavelength range of 300–900 nm as shown in Fig. 7a. It can be found that oxidation treatment reduced the light transmittance of the membrane compared to the CM. Comparative speaking, the introduction of PEI and C–Cl bond improved the transparency of the membrane. In four samples, the transmittance of the Cl–PEI–DCM was the highest. From the inset of Fig. 7a, the transparency and flexibility of the Cl–PEI–DCM can be visually observed. At the same time, the mechanical properties of the Cl–PEI–DCM was tested, and the tensile strength and elongation at break were given in Fig. 7b. It can be seen that there were evident reduces of about 13% for the tensile strength (from 130.12 to 112.80 MPa) and 15% for the elongation at break (from 9.63 to 8.20%) at the oxidation stage. Afterward, a slow decrease was observed for the tensile strength at graft and chlorination stages. In contrast, a remarkable enhancement of about 38% for the elongation at break (from 8.20 to 11.33%) can be realized after the introduction of PEI. The Cl–PEI–DCM still remained a high tensile strength of 105 MPa and elongation at break of 10.10%.

Antibacterial activity

The antibacterial efficacy of the PEI–DCM and 1.30 wt% Cl–PEI–DCM were determined with Gram-positive bacteria *S. aureus* and Gram-negative bacteria *E. coli* and the results were showed in Table 1. It can be seen clearly that the chlorinated sample exhibited high antibacterial efficacy against both bacterial species, which can completely inactivate all of *S. aureus* and *E. coli* within 5 min even after 15 days of storage. When shortening the contact time from 5 to 1 min, it still provided higher than 99.50% reduction for *S. aureus* and for *E. coli* after 30 days of storage. By comparison, the PEI–DCM had low reduction of bacteria concentration, which only provided 36.00% reduction of *S. aureus* and 21.40% of *E. coli* within 30 min, respectively. Hence, the Cl–PEI–DCM can be applied as a potential wound dressing. Recently, the paper published by the Worley group has demonstrated that N-halamine wound dressings potentially can be employed to prevent infections (Buket et al. 2017). The strong antibacterial efficacy of the Cl–PEI–DCM was related to the direct transfer of oxidative Cl(+I) from N-halamines to microbial cell walls. This process can rupture receptors in the cell, destroy or inhibit the enzymatic or metabolic process, and inactivate the organisms (Li et al. 2015).

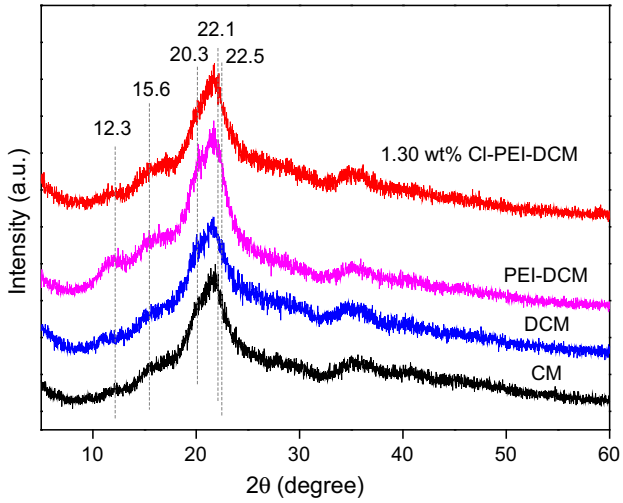

Fig. 6 XRD patterns of the CM, DCM, PEI–DCM and 1.30 wt% Cl–PEI–DCM

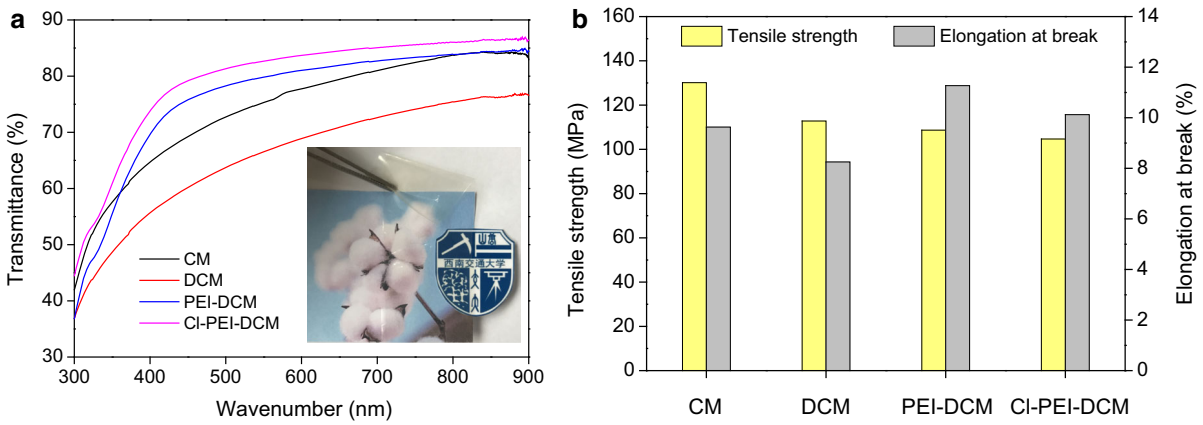

Fig. 7 The transparency (**a**) and mechanical properties (**b**) of the samples prepared at different stages

Table 1 Antibacterial efficacy of the PEI–DCM and 1.30 wt% Cl–PEI–DCM to bacteria *S. aureus* and *E. coli*

Sample	Contact time (min)	*S. aureus* reduction (%)	*E. coli* reduction (%)
PEI–DCM	30	36.00	21.42
1.30 wt% Cl-PEI-DCM			
The 1st day	1	99.82	99.56
(Exp 1[a])	5	100 (no growth)	100 (no growth)
The 1st day	1	99.92	99.85
(Exp 2[a])	5	100 (no growth)	100 (no growth)
The 1st day	1	99.97	99.74
(Exp 3[a])	5	100 (no growth)	100 (no growth)
The 15th day	1	99.76	99.53
	5	100 (no growth)	100 (no growth)
The 30th day	1	99.64	99.51
	5	99.94	99.90

[a]Data represented two different experiments being performed on different days with different inoculum populations. For Exp 1, the inoculum population was 5.4×10^6 CUF/mL for *S. aureus* and 4.3×10^6 for *E. coli*. For Exp 2, the inoculum population was 3.6×10^6 CUF/mL for *S. aureus* and 8.7×10^6 for *E. coli*. For Exp 3, the inoculum population was 8.5×10^6 CUF/mL for *S. aureus* and 7.9×10^6 for *E. coli*

Stability and rechargeability of the Cl–PEI–DCM

The stability and rechargeability of the Cl–PEI–DCM were evaluated and the results were presented in Fig. 8. Though the Cl^+ content of the tested samples gradually decreased with the increase of storage time, about 77% of the initial chlorine loading was still retained after 30 days of storage. When combined with the antibacterial efficacy result, this stability is enough to support its application. The loss of chlorine could be caused by hydrolysis of N–Cl bonds (Liu et al. 2015).

From Fig. 8, the rechargeability of the Cl–PEI–DCM was confirmed via an iodometric/thiosulfate titration. After three dechlorination/chlorination cycles, more than 70% of oxidative chlorine content can be recovered. This result indicated that the Cl–PEI–DCM had good rechargeability.

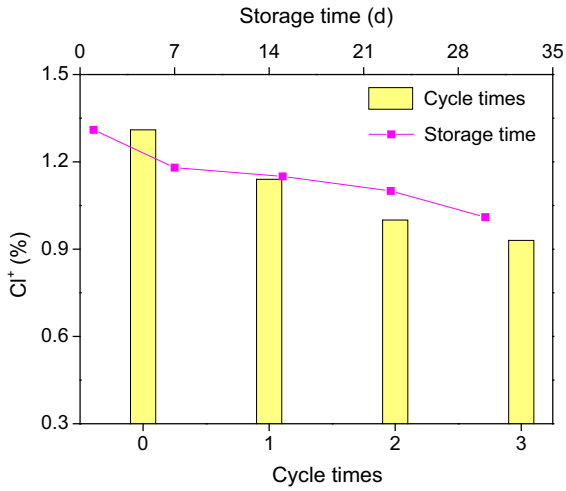

Fig. 8 Stability and rechargeability of the Cl–PEI–DCM

Conclusion

A novel N-halamine antibacterial cellulose membrane was successfully fabricated via grafting PEI onto dialdehyde cellulose followed by chloramination. The appropriate conditions affecting the aldehyde content of DCM and the active chlorine (Cl^+) content of Cl–PEI–DCM were systematically investigated at oxidation, grafting and chlorination stages, respectively. Results showed that the Cl^+ content of Cl–PEI–DCM was strongly dependent on the aldehyde content of DCM and PEI concentration. Under the optimum testing condition, the Cl^+ content of the resultant product reached 1.30 wt%. ATR–FTIR and XPS results indicated that the hydroxyl groups on the CM were changed to aldehyde groups. The PEI was successfully grafted onto the surface of DCM, where the primary amino and secondary amino groups were preserved. After chlorination, the N–Cl bonds were successfully introduced to the surface of Cl–PEI–DCM. Compared with the PEI–DCM, the chlorinated sample 1.30 wt% Cl–PEI–DCM exhibited high antibacterial efficiency against *S. aureus* and *E. coli*. They can completely inactivate two bacterial pathogens within 5 min even after 15 days of storage. Moreover, the Cl–PEI–DCM displayed good stability, rechargeability, transparency and high mechanical strength, which can be considered as a visualized wound dressing material or antibacterial shoe insole.

Acknowledgments The present work financially supported by Science and Technology Pillar Program of Sichuan Province (2016GZ0222).

References

Bastarrachea LJ, Goddard JM (2013) Development of antimicrobial stainless steel via surface modification with N-halamines: characterization of surface chemistry and N-halamine chlorination. J Appl Polym Sci 127:821–831

Buket D, Roy B, Mingyu Q, Tung-Shi H, Worley S (2017) N-halamine biocidal materials with superior antimicrobial efficacies for wound dressings. Molecules 22(10):1582–1598

Cao J, Wei W, Gou GJ, Jiang M, Cui YH, Zhang SL, Wang Y, Zhou ZW (2018) Cellulose films from the aqueous DMSO/TBAH-system. Cellulose 25:1975–1986

Chen YX, Li JN, Li QQ, Shen YY, Ge ZC, Zhang WW, Chen SG (2016) Novel water-soluble, antibacterial, and biocompatible quaternized chitosan by introducing sulfobetaine. Carbohydr Polym 143:246–253

Chen SG, Zhang SB, Galluzzi M, Li F, Zhang XC, Yang XH, Liu XY, Cai XH, Zhu XL, Du B, Li JN, Huang P (2019) Insight into multifunctional polyester fabrics finished by one-step ecofriendly strategy. Chem Eng J 358:634–642

Cheung RCF, Ng TB, Wong JH, Chan WY (2015) Chitosan: an update on potential biomedical and pharmaceutical applications. Mar Drugs 13(8):5156–5186

Ciofani G, Raffa V, Menciassi A, Cuschieri A (2008) Cytocompatibility, interactions, and uptake of polyethyleneimine-coated boron nitride nanotubes by living cells: confirmation of their potential for biomedical applications. Biotechnol Bioeng 101:850–858

Deborde M, von Gunten U (2008) Reactions of chlorine with inorganic and organic compounds during water treatment—kinetics and mechanisms: a critical review. Water Res 42(1–2):13–51

Demir B, Broughton RM, Huang TS, Bozack MJ, Worley SD (2017) Polymeric antimicrobial N-halamine-surface modification of stainless steel. Ind Eng Chem Res 56:11773–11781

Demircan D, Zhang BZ (2017) Facile synthesis of novel soluble cellulose-grafted hyperbranched polymers as potential natural antimicrobial materials. Carbohydr Polym 157:1913–1921

Dong A, Wang YJ, Gao YY, Gao TY, Gao G (2017) Chemical insights into antibacterial N-halamines. Chem Rev 117:4806–4862

Gerba CP (2015) Quaternary ammonium biocides: efficacy in application. Appl Environ Microbiol 81(2):464–469

Gu JW, Yuan LJ, Zhang Z, Yang XH, Luo JX, Gui ZF, Chen SG (2018) Non-leaching bactericidal cotton fabrics with well-preserved physical properties, no skin irritation and no toxicity. Cellulose 25:5415–5426

Hou SH, Dong X, Zhu JH, Zheng JF, Bi WH, Li SH, Zhang SB (2017) Preparation and characterization of an antibacterial ultrafiltration membrane with N-chloramine functional groups. J Colloid Interface Sci 496:391–400

Hui F, Debiemme-Chouvy C (2013) Antimicrobial N-halamine polymers and coatings: a review of their synthesis, characterization, and applications. Biomacromolecules 14(3):585–601

Jin LQ, Li WG, Xu QH, Sun QC (2015) Amino-functionalized nanocrystalline cellulose as an adsorbent for anionic dyes. Cellulose 22:2443–2456

Kang ZZ, Zhang B, Jiao YC, Xu YH, He QZ, Liang J (2013) High-efficacy antimicrobial cellulose grafted by a novel quaternarized N-halamine. Cellulose 20(2):885–893

Kang B, Li YD, Liang J, Yan X, Chen J, Lang WZ (2016) Novel PVDF hollow fiber ultrafiltration membranes with antibacterial and antifouling properties by embedding N-halamine functionalized multiwalled carbon nanotubes (MWNTs). RSC Adv 6:1710–1721

Kim UJ, Kuga S, Wada M, Okano T, Kondo T (2000) Periodate oxidation of crystalline cellulose. Biomacromolecules 1:488–492

Li HL, Wu B, Mu CD, Lin W (2011) Concomitant degradation in periodate oxidation of carboxymethyl cellulose. Carbohydr Polym 84:881–886

Li L, Puhl S, Meinel L, Germershaus O (2014) Silk fibroin layer-by-layer microcapsules for localized gene delivery. Biomaterials 35:7929–7939

Li XL, Liu Y, Jiang ZM, Li R, Ren XH, Huang TS (2015) Synthesis of an N-halamine monomer and its application in antimicrobial cellulose via an electron beam irradiation process. Cellulose 22(6):3609–3617

Lindh J, Carlsson DO, Strømme M, Mihranyan A (2014) Convenient one-pot formation of 2,3-dialdehyde cellulose beads via periodate oxidation of cellulose in water. Biomacromolecules 15:1928–1932

Liu Y, Li J, Cheng X, Ren X, Huang TS (2015) Self-assembled antibacterial coating by N-halamine polyelectrolytes on a cellulose substrate. J Mater Chem B 3:1446–1454

Parhiz H, Hashemi M, Hatefi A, Shier WT, Farzad SA, Ramezani M (2013) Arginine-rich hydrophobic polyethylenimine: potent agent with simple components for nucleic acid delivery. Int J Biol Macromol 60:18–27

Qi KZ, Cheng B, Yu JG, Ho WK (2017) Review on the improvement of the photocatalytic and antibacterial activities of ZnO. J Alloys Compd 27:792–820

Roy D, Semsarilar M, Guthrie JT, Perrier S (2009) Cellulose modification by polymer grafting: a review. Chem Soc Rev 38(7):2046–2064

Shankar S, Rhim JW (2018) Antimicrobial wrapping paper coated with a ternary blend of carbohydrates (alginate, carboxymethyl cellulose, carrageenan) and grapefruit seed extract. Carbohydr Polym 196:92–101

Sheppard NC, Brinckmann SA, Gartlan KH, Puthia M, Svanborg C, Krashias G, Eisenbarth SC, Flavell RA, Sattentau QJ, Wegmann F (2014) Polyethyleneimine is a potent systemic adjuvant for glycoprotein antigens. Int Immunol 26:531–538

Soice NP, Maladono AC, Takigawa DY, Norman AD, Krantz WB, Greenberg AR (2003) Oxidative degradation of polyamide reverse osmosis membranes: studies of molecular model compounds and selected membranes. J Appl Polym Sci 90(5):1173–1184

Sun YY, Chen TY, Worley SD, Sun G (2001) Novel refreshable N-halamine polymeric biocides containing imidazolidin-4-one derivatives. J Polym Sci Polym Chem 39(18):3073–3084

Toure Y, Genet MJ, Dupont-Gillain CC, Sindic M, Rouxhet PG (2014) Conditioning materials with biomacromolecules: composition of the adlayer and influence on clean ability. J Colloid Interface Sci 432:158–169

Varma AJ, Kokane SP, Pathak G, Pradhan SD (1997) Thermal behavior of galactomannan guar gum and its periodate oxidation products. Carbohydr Polym 32(2):111–114

Wang H, Wang ZM, Yan X, Chen J, Lang WZ, Guo YJ (2017a) Novel organic-inorganic hybrid polyvinylidene fluoride ultrafiltration membranes with antifouling and antibacterial properties by embedding N-halamine functionalized silica nanospheres. J Ind Eng Chem 52:295–304

Wang LL, Hu C, Shao LQ (2017b) The antimicrobial activity of nanoparticles: present situation and prospects for the future. Int J Nanomed 12:1227–1249

Zhang XY, Shen GY, Sun SY, Shen YM, Zhan CXG, Xiao AG (2014) Direct immobilization of antibodies on dialdehyde cellulose film for convenient construction of an electrochemical immunosensor. Sens Actuators B Chem 200:304–309

Zhang SL, Wang ZK, Chen HY, Kai CC, Jiang M, Wang Q, Zhou ZW (2018) Polyethylenimine functionalized Fe_3O_4/steam-exploded rice straw composite as an efficient adsorbent for Cr(VI) removal. Appl Surf Sci 440:1277–1285